MIT Open Access Articles

DNA-Directed Non-Langmuir Deposition of Programmable Atom Equivalents

DNA-Directed Non-Langmuir Deposition of Programmable Atom Equivalents

AUTHOR NAMES. Diana J. Lewis[‡], Paul A. Gabrys[†], and Robert J. Macfarlane[*,†]

AUTHOR ADDRESS.

‡Draper, 555 Technology Square, Cambridge, Massachusetts 02139, and Department of Aeronautics and Astronautics, †Department of Materials Science and Engineering, Massachusetts Institute of Technology (MIT), 77 Massachusetts Avenue, Cambridge, Massachusetts 02139, United States

*Address correspondence to rmacfarl@mit.edu

KEYWORDS. Nanoparticle, DNA, Self-Assembly, Thin Film, Deposition, Adsorption, Langmuir, Random Sequential Adsorption

ABSTRACT. Particle assembly at interfaces via programmed DNA interactions allows for independent modification of both nanoparticle-surface interaction strength and the magnitude of interparticle repulsion. Together, these factors allow for modification of the deposited thin film morphology via alterations in DNA binding sequence. Importantly, both Langmuir and random sequential adsorption models yield insights into the thermodynamics of deposition, but cannot fully explain particle coverage as a function of all relevant variables, indicating that the particle

deposition mechanism for DNA-grafted colloids is more complex than prior adsorption phenomena. Here, it is shown that these deviations from standard behavior arise from the fact that each nanoparticle is attached to the surface via multiple weak DNA duplex interactions, enabling diffusion of adsorbed colloids across the substrate. Thus, surface migration of individual particles causes reorganization of the deposited monolayer, leading to the unusual behavior of coverage *increasing* at elevated temperatures that are just below the particle desorption temperature. The programmability of DNA-directed particle deposition therefore allows for precise control over the morphology of monolayer films, as well as the ability to generate crystalline materials with controllable surface roughness and grain size through layer-by-layer growth. The increased control over thin film morphology potentially enables tailoring of mechanical and optical properties, and holds promise for use in a variety of applications.

TEXT.

Introduction

Nanoparticle-based thin films are a unique class of material with potential utility in a variety of diverse applications, including optical devices[1], surfaces with enhanced hydrophilicity[2,3], and biosensing[4]. In order to fabricate a functional film using nanoparticles as building blocks, however, the synthesis method being used must be capable of controlling the morphology of the film, including factors related to both particle design (size, shape, and composition), as well as the arrangement of particles on the surface (interparticle spacing, long range ordering, crystallographic symmetry)[5,6]. This poses a challenge for many common deposition processes, which are unable to fully manipulate all of these design factors[7]. For example, Langmuir-Blodgett and similar techniques rely on external forces to close-pack particles as they are deposited, limiting their ability to generate non-close packed structures without further processing[8,9]. Simple drop casting or

immersion methods that use uncontrolled electrostatic or van der Waals forces to drive particle assembly commonly result in a random arrangement of particles, with little control over particle positions or interparticle spacings[10]. In addition, interparticle potentials that can alter spacing are inherently linked to the particle-surface interactions in those systems; decreasing interparticle repulsion also reduces the particles' affinity for the surface. The most tailorable strategies for particle thin film deposition use small molecule directing ligands grafted to the surface of each nanoparticle in order to tune interparticle potentials, and thus an ideal ligand would possess readily understood and manipulated design handles that allow for complete manipulation of the structural factors that affect thin film physical properties.

Although multiple strategies have been developed to control thin film synthesis using a variety of different ligands[11–14], DNA is an ideal choice for directing thin film assembly, as interactions between DNA strands can be precisely controlled as a function of their nucleotide sequence[5,15]. By coating a substrate with a brush of oligonucleotides, particle assembly on that surface can be easily regulated by functionalizing a set of particles with the complementary sequence, allowing the particles to form DNA-based bonds with the oligonucleotide brush. This assembly strategy can be used to generate particle monolayers. Particle multilayers can subsequently be formed by alternately exposing the surface to complementary particle types, building a film through layer-by-layer deposition[5,15]. Previous work has even shown that crystalline, body centered cubic (bcc) lattices can be grown from substrates if the deposition conditions (e.g. temperature, particle design) are appropriately controlled[5]. In addition, solution-phase crystallization of nanoparticles functionalized with DNA, dubbed 'programmable atom equivalents' (PAEs), has shown that an array of crystal structures can be generated simply by altering PAE design[16–18], suggesting that many more thin film morphologies can also be achieved via judicious selection of DNA sequences.

However, while PAE deposition has been demonstrated as a viable means to control particle ordering in both colloidal suspensions and thin film architectures[15,19–25], the deposition process has not been optimized to produce thin films with defined amounts of both surface coverage and tailorable particle arrangements. Here we investigate how altering multiple design factors and assembly conditions affect the thermodynamics of PAE deposition, as well as the resulting film morphology. Specifically, we examine the effects of DNA binding strength, solution ionic strength, and deposition temperature on the surface coverage and distribution of nanoparticles in a monolayer. In addition, we explore how the structure of an initial monolayer affects the subsequent deposition of bilayer and multilayer films. Interestingly, we show that the deposition process exhibits unexpected phenomena that cannot be explained by previous simple models of deposition, but can be explained as a function of the unique PAE architecture and its ability to reorganize upon thermal annealing. This work demonstrates that PAEs can be employed to control film morphology and surface coverage by tuning the DNA binding strength, ionic strength and temperature. Furthermore, this work elucidates the mechanisms that control thin film structure, creating a framework for the design of specific architectures needed in the aforementioned applications.

Materials and Methods

Full experimental procedures for all depositions and analyses of the materials examined in this work can be found in the supporting information (SI). Samples were produced by first synthesizing nominally 20 nm diameter gold nanoparticles using an established literature protocol[26], and both these particles and gold-coated quartz substrates were subsequently functionalized with thiol-terminated DNA strands (details described in SI)[27]. These thiol-terminated "anchor" strands were

then hybridized with DNA "linkers" at a ratio of 0.8 linker strands per anchor strand, forming rigid DNA duplexes that presented a short 6-base (standard) or 10-base (long) "sticky end" sequence at their termini (full sequences can be found in the SI, Table S1). Hybridization between DNA linkers on the substrate and linkers attached to PAEs occurred when their respective sticky ends were complementary to one another. After functionalization with both anchor and linker strands, PAEs were diluted to the relevant concentration for each deposition experiment (0.05 – 1 nM) in phosphate buffered saline (PBS, [NaCl] = 0.1 – 0.5 M).

Substrates were prepared by e-beam deposition (ATC-E series, AJA International, Inc) of 2 nm chromium (0.2 Å/sec), then 8 nm gold (0.2 Å/sec) onto solvent cleaned quartz slides (Ted Pella). The quartz slides were diced using a die saw into 7.5 mm x 12.5 mm substrates, which were subsequently functionalized as discussed above. At least three substrates were used per experimental condition to ensure statistical relevance of all measurements.

Deposition experiments were performed by incubating the substrates in temperature controlled containers of the appropriate PAE solution, stirred during deposition to ensure homogeneity (details in SI). After deposition was complete, substrates were removed from solution and rinsed in PBS. Surface coverage was determined via changes in the UV-vis absorption of the nanoparticle thin film at 520 nm (Agilent Cary 5000). Nanoparticle deposition at the lowest concentration equilibrated after two days. Therefore, all substrates in the concentration vs. coverage experiments were incubated in their respective solutions for three days to ensure equilibrium coverage. All other experiments used a 0.5 nM PAE concentration and an incubation time of five hours, which was noted to exceed the equilibration time for a 0.5 nM solution (See SI). Appropriate solution volumes were used to ensure the particle concentration did not decrease by more than 10% during deposition. Multilayer films were produced by functionalizing two sets of PAEs with

complementary linkers, and successively immersing substrates in alternating solutions of the two PAE types. Full deposition protocols and conditions for all films are listed in the SI.

After deposition, the temperature at which PAEs desorbed from the films was measured by placing the substrates in solutions of PBS, and monitoring UV-vis absorption at 520 nm while ramping the temperature slowly at a rate of 0.25 °C/min from 20 °C to 65 °C.

Scanning electron microscope (SEM) images (Zeiss Supra 35VP) of PAE thin films were obtained by first embedding the samples in silica[28], followed by removal of all solvent. Images were analyzed with ImageJ to obtain a particle count, which was then correlated to coverage using the average diameter of a PAE in solution (see SI for details). The UV-vis absorption for all substrates was converted to coverage by using a conversion factor derived from the comparison between the SEM coverage and the absorption. Atomic Force Microscopy (AFM) (Bruker Dimension Fastscan, Icon head) images were taken of bilayer and five-layer samples to obtain surface morphology and roughness. An 8 nm nominal radius SNL-B cantilever was used for imaging.

Results

PAEs are a uniquely tailorable system for thin film deposition, with multiple design handles that can be used to tune the strength of their interactions with the substrate. The relevant variables include particle core size, DNA linker length, number of DNA linkers per particle, and the overall strength of each sticky end duplex. Together, these variables dictate how tightly each PAE binds to a DNA-coated substrate by manipulating the multivalency of that interaction. Additionally, ambient conditions such as temperature and solution ionic strength have been shown to affect PAE-PAE binding in solution[29], and therefore provide additional handles to control the deposition

of PAEs onto a substrate. Due to the large design space that can be explored, prior models for colloidal deposition were first examined to determine which of the variables discussed above would be most relevant for controlling thin film morphology, specifically the Langmuir model and the Random Sequential Adsorption (RSA) model.

Comparison of RSA and Langmuir Adsorption Models

The Langmuir model, a simple two-parameter equation derived from first principles, is commonly used to describe adsorption processes of atomic species, and has been used to model and extract thermodynamic parameters in a similar PAE system[30]. This model is based on the assumption that particles are free to both adsorb and subsequently desorb from the surface, and equilibrium coverage is reached when the rates of adsorption and desorption are balanced. Coverage (θ) can therefore be expressed as eq 1:

$$\theta = \frac{KP}{1+KP} \qquad (1)$$

where K is the equilibrium constant of the adsorption process (eq 2) and P is the concentration of nanoparticles in solution[31].

$$K = \frac{k_{ads}}{k_{des}} \qquad (2)$$

For PAEs, the rate constant for adsorption (k_{ads}) and the rate constant for desorption (k_{des}) are expected to be linked respectively to the rate constants of hybridization (k_{on}) and dehybridization (k_{off}) of individual DNA strands[29,32]. k_{on} has been shown to be weakly temperature dependent[33], while the dehybridization rate constant (k_{off}) increases proportional to

$$k_{off} \propto e^{\left(\frac{-\Delta G}{k_B T}\right)} \qquad (3)$$

where ΔG is the Gibbs free energy of hybridization of the DNA, k_B is the Boltzmann constant, and T is solution temperature[29]. The Langmuir model therefore predicts that coverage will decrease

with increasing temperature and increase with increasing particle concentration. While this model provides a simple means of calculating surface coverage, key assumptions render it unable to fully and accurately describe the PAE deposition process. Specifically, the equations above are only valid for systems with a set number of independent, equivalent adsorption sites, where adsorbates are immobilized once bound to the surface and do not interact with one another. However, the PAE system consists of nanoparticles coated with polyanionic brushes that lead to significant repulsion between PAEs at close distances, and the polymer brush coating on the substrates provide a continuous surface on which these PAEs can bind.

In contrast to the Langmuir model, the RSA model for colloidal deposition utilizes complex numerical methods to simulate colloid adsorption processes by sequentially and permanently affixing hard spheres to random positions on a continuous surface[34]. The Derjaguin-Landau-Verwey-Overbeek (DLVO) theory that incorporates electrostatic repulsion and van der Waals forces is commonly used to model particle-surface interactions, and model inputs can be adjusted to account for different interparticle and particle-surface interactions[35]. However, because the RSA model assumes that particles cannot migrate or desorb once bound, it always predicts a maximum 'jamming' coverage of 0.547 for spheres on a flat plane[36], where all of the remaining surface area consists of spaces too small for another particle to land. Because PAE-substrate binding is dynamic and temperature dependent (as indicated by the fact that PAEs will melt off a surface at elevated temperatures), the irreversible adsorption assumption is clearly violated for this system, particularly at temperatures nearing the melting temperature. As a result, neither RSA nor Langmuir deposition models can be expected to fully and accurately describe PAE deposition. However, examination of the PAE system in context of one or both of these models could provide useful insights into deposition behavior, particularly with respect to the effects of deposition

parameters such as solution ionic strength, solution temperature, and particle-surface interaction strength. Therefore, maximum PAE coverage was first examined as a function of these variables, and compared to predicted coverage based on Langmuir and RSA models.

Effects of PAE Concentration on Coverage

PAE substrate coverage as a function of concentration under standard conditions (0.5 M PBS, 22 °C), was found to be independent of the concentration over the accessible range (see SI), with an average fractional surface coverage of 0.681 (Figure 1). Importantly, this coverage value is determined as PAE coverage, not gold nanoparticle coverage - in other words, the amount of surface area occupied by each PAE consists of the area occupied by both the gold nanoparticle core and the DNA corona that surrounds it. Additionally, substrates were re-measured after ten days of immersion in pure (PAE-free) PBS at room temperature and found to have no discernable drop in coverage. This stability indicates that the desorption rate of this particular PAE design under the standard conditions noted above is negligible. This behavior is consistent with the permanent adsorption assumption of the RSA model, suggesting its utility in studying the system in this regime. It is important to note that the RSA model typically predicts a maximum surface coverage of 0.547, below the experimental results. The observed difference is likely due to the compressibility of the DNA coronae. The coverage values are calculated assuming the PAE size in solution when the DNA is fully extended and not hybridized to a surface or adjacent PAE (see SI). However, the DNA length calculated from the interparticle distances within a PAE crystal in 0.5 M PBS is 21% smaller than the value for an nonbound PAE (see SI). These PAEs are not in a lattice and therefore not expected to be uniformly compressed, but it is likely that they are able to deform a significant amount, allowing more particles to adsorb than predicted from the hard sphere

model. While this deformability is difficult to measure experimentally, prior experimental and computational evidence has demonstrated that even "rigid" DNA duplexes are capable of significant deformation in solution[39,40], meaning that the "effective" diameter of the bound PAEs is expected to be smaller than the diameter of PAEs free in solution. Additionally, if the presence of a compressible DNA corona did indeed affect the effective PAE diameter, it would be expected that the surface coverage would increase for PAEs functionalized with longer DNA strands, due to their greater ability to deform; additional experiments (see SI) show that coverage does increase for PAEs with longer DNA.
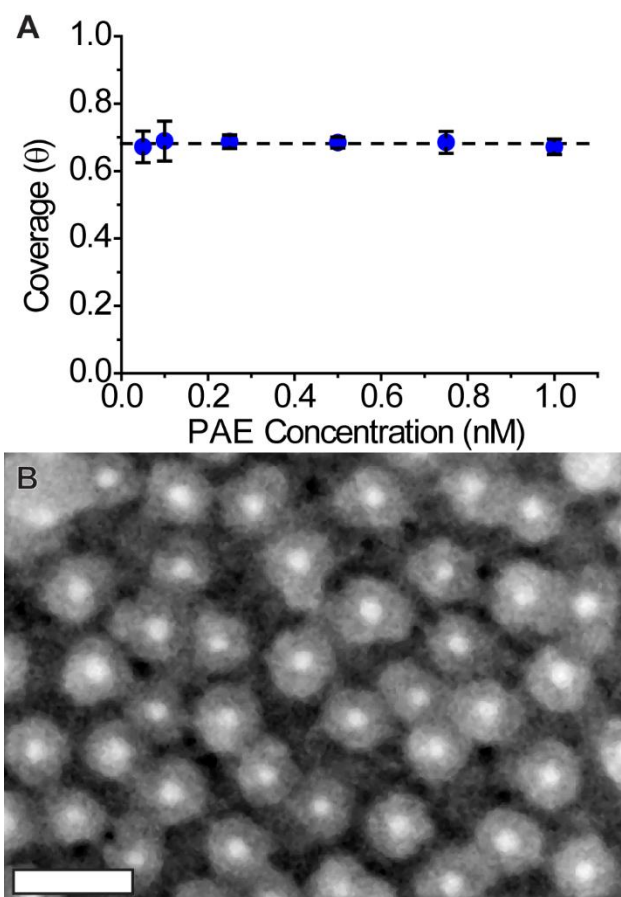
Figure 1. (A) Coverage as a function of PAE concentration, showing that coverage is independent of concentration. Error bars are 95% confidence intervals. (B) SEM image of a substrate with a coverage of 0.681. Scale bar is 100 nm.

Effects of Ionic Strength on Coverage

While the data above shows that PAE coverage cannot be modified with concentration at room temperature, the ionic concentration of the solution would be predicted to affect coverage by modulating interparticle electrostatic repulsion. Indeed, when the NaCl concentration was reduced, the coverage decreased, indicating that the effective interaction range for interparticle repulsion had increased. This interaction range can be approximated as the Debye length[35], which depends on ionic concentration following the formula

$$\kappa^{-1} = \sqrt{\frac{\epsilon_r \epsilon_0 k_B T}{2 N_A e^2 I}} \quad (4)$$

where ϵ_r is the dielectric constant, ϵ_o is the permittivity of free space, k_B is the Boltzmann constant, T is the absolute temperature in K, N_A is Avogadro's number, e is the elementary charge and I is the ionic strength of the solution. Therefore, as the thickness of the electrical double layer increases, it increases the effective radius of a nanoparticle due to greater interparticle repulsion, resulting in each PAE blocking a greater fraction of the surface and reducing the overall surface coverage. The RSA model can be modified to predict the PAE coverage as a function of this effective radius following

$$\theta = \theta_{max} \left(\frac{r}{r_{eff}} \right)^2 \quad (5)$$

where r is the particle radius, and the effective radius, r_{eff}, is equal to r plus $c\kappa^{-1}$, where c is a proportionality constant (see SI, eq S3). Substituting to relate coverage to ionic strength directly yields

$$\theta = \theta_{max} \frac{1}{\left(1 + \dfrac{a}{\sqrt{I}} \right)^2} \quad (6)$$

where *a* is a fit parameter incorporating the nanoparticle radius, the constants in the Debye equation, and the proportionality constant. The experimental data can be fit to this two-parameter model to yield a hypothetical maximum coverage and predict coverage for other ionic concentrations, Figure 2.
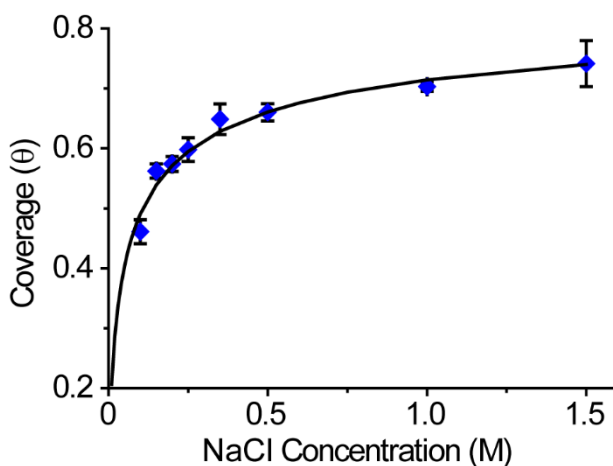

Figure 2. Coverage as a function of NaCl concentration (half of the ionic strength). Line shows coverage prediction from eq 6, where $\theta_{max} = 0.873$ and a = 0.150. Error bars are 95% confidence intervals.

Effects of Temperature on Coverage

While the RSA model proves useful for predicting coverages at room temperature, it cannot be expected to work at elevated temperatures where PAE binding becomes reversible. The obvious expectation is therefore that surface coverage would decrease as the temperature of the deposition solution is raised, generating a temperature-dependent coverage profile that is better described by the Langmuir model. However, while there was indeed a drop in coverage for solutions deposited above the observed PAE melting temperature, at temperatures immediately below this transition, coverage actually *increased* relative to the room temperature deposited films (Figure 3, statistical analysis in SI). This unexpected behavior is contrary to both the Langmuir and RSA models, and

is actually inverse to the expected behavior from eq 4, which suggests that increasing temperature should increase the PAE interaction range thereby decreasing coverage. This temperature dependence has not been shown in previous methods that deposit colloids from a liquid suspension; in fact, temperature is often not even noted as a parameter that can be used to alter coverage[41,42]. The observed increase in coverage in this PAE system at these elevated temperatures is hypothesized to arise from the distinctive ability of PAEs to reorganize at moderate temperatures due to the fact that they are bound to the surface via multiple weak DNA duplex interactions[29]. Because PAEs attach to the surface with many weak connections that can individually hybridize/dehybridize without completely breaking the overall bond between the PAE and the surface, at moderately high temperatures, enough individual connections can be in a state of flux such that a PAE can become mobile without fully desorbing from the surface[21]. This migration of adsorbed PAEs opens up previously blocked surface area, allowing more particles to adsorb, leading to increased surface coverage.
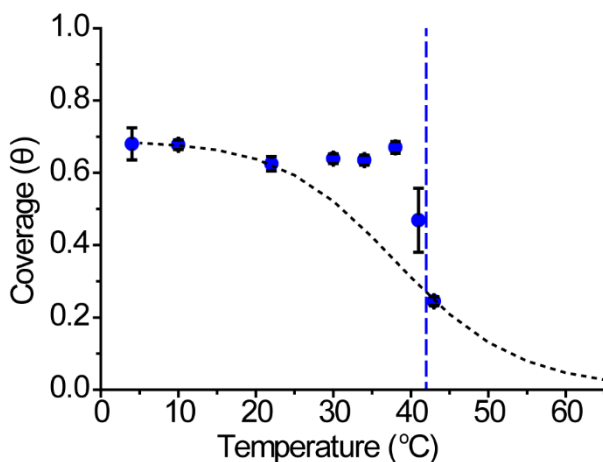
Figure 3. Coverage as a function of temperature. Note that as temperature increases, there is a rise in the coverage that occurs at temperatures approaching the melting temperature (vertical dashed line). Black line shows a fit to the standard Langmuir model, highlighting the deviation from typical Langmuir behavior. Error bars are 95% confidence intervals.

13

Importantly, this reorganization behavior implies that it should be possible to modify the adsorption conditions not only to modulate thin film coverage, but also film morphology and particle ordering on the surface. These changes should in principle be achievable by altering design parameters that affect both the temperature at which desorption occurs and the overall thermal breadth of the PAE melting and desorption transition. Specifically, the most critical factors to alter PAE deposition without significantly modifying the overall structure of the PAE (in terms of nanoparticle core size or DNA linker length) would therefore be the ionic strength of the solution and the base sequence of the linker sticky ends.

Combined Effects of Temperature, Ionic Strength and Linker Sticky End Design on Coverage

Because the backbone of each DNA strand is polyanionic, lowering the ionic concentration of the solution results in greater interstrand repulsion. In standard DNA duplexes, this lowers the free energy of duplex formation and slows the kinetics of association for complementary DNA sequences. In the system analyzed here where each DNA-based bond between PAEs and the substrate consists of multiple weak and dynamic sticky end duplexes, these alterations to duplex formation behavior should lead to PAEs desorbing from the surface at lower temperatures, as well as a narrowed range of temperatures at which PAEs are adsorbed to the surface but still mobile[29].

To test this hypothesis, PAEs were suspended in reduced ionic strength environments (0.15 M PBS, compared with the standard 0.5 M PBS of prior experiments), and deposited at various temperatures (Figure 4). As expected, the melting temperature of this system was indeed depressed and the overall coverage at all temperatures decreased due to increased interparticle repulsion and decreased strength of the PAE-substrate interactions, consistent with eq 4 and eq 6 and prior experiments[29]. Additionally, the thermal window over which reorganization of adsorbed PAEs

enabled higher surface coverage significantly narrowed, and deviation from standard Langmuir-predicted behavior was observed only immediately below the melting transition. Interestingly, the relative enhancement of coverage at these temperatures was greater than the observed enhancement for the higher ionic strength depositions. This difference is hypothesized to arise from a combination of increased mobility due to the lower overall surface coverage as well as lower surface affinity (due to increased repulsion).

In addition to modifying PAE-substrate binding via alterations to solution ion concentration, it is possible to alter the strength of the dynamic, multivalent bonds by changing the base sequence of the DNA sticky ends. It is important to note that the sticky end duplexes that form when PAEs bind to the substrate are significantly shorter than the overall length of the DNA linkers (6 base sticky ends on 67 base linker strands). This means that minor alterations to sticky end sequence should have minimal effect on the overall size of a PAE and also minimal effect on interparticle repulsion, but should have significant impact on the overall strength of a PAE-substrate bond. In order to examine the effects of altering PAE binding in this manner, the sticky end sequence was increased from 6 to 10 bases, nearly doubling the strength of an individual sticky end interaction (ΔG_{hyb} from -42.4 kJ/mol to -77.2 kJ/mol). This alteration means that while the 6-base duplex is dynamic under standard deposition conditions (22 °C), the 10-base duplex is essentially permanently bound at this temperature. Because PAE reorganization requires multiple weak sticky end interactions continuously associating and dissociating[32], increasing the individual strands' melting temperature to this level was hypothesized to prevent any rearrangement at standard deposition temperature. Additionally, by using such a strong individual strand interaction, it was expected that the reorganization window would narrow to such a degree that it would be entirely convoluted with the dissociation of the PAEs from the surface, virtually eliminating the

reorganization window. Thus, any increase in adsorption from particles moving to accommodate more PAEs would be entirely canceled by the increase in desorption from being so near to the melting temperature.

As hypothesized, melting for this 10-base sticky end system occurs at a higher temperature than the standard case. Moreover, as temperature increases, coverage begins to deviate from Langmuir behavior at a temperature four degrees below the melting temperature (Figure 4). Above this temperature, a dramatic spike in the adsorption curve appears, reaching a maximum coverage of 0.91, a 52% increase over the minimum coverage that occurred six degrees lower. It is important to note that this maximum was reached two degrees above the measured melting temperature; because the melting temperature of the monolayer film is determined in a solution without excess PAEs, it was likely lower than the melting temperature of the deposition solution which possessed a large reservoir of nanoparticles that could readsorb (see further discussion in the SI). This melting temperature increase has been observed in previous solution-phase work, which contrasted a quiescent measurement with one that involved stirring[29]. It is, however, unexpected that the adsorption rate would exceed the desorption rate in this regime, as the rate constant for DNA hybridization has been determined to be nearly invariant with temperature, while the rate constant for dehybridization increases exponentially with temperature[29,33]. The increase in coverage at these elevated temperatures can therefore be best explained by the surface reorganization processes discussed above, and not any inherent changes to the rates of adsorption or desorption. This hypothesis is further supported by prior examinations of PAE crystallization in solution-phase work[29], where reorganization occurs in an 'annealing window' comparable in breadth and relation to the melting temperature in this work.
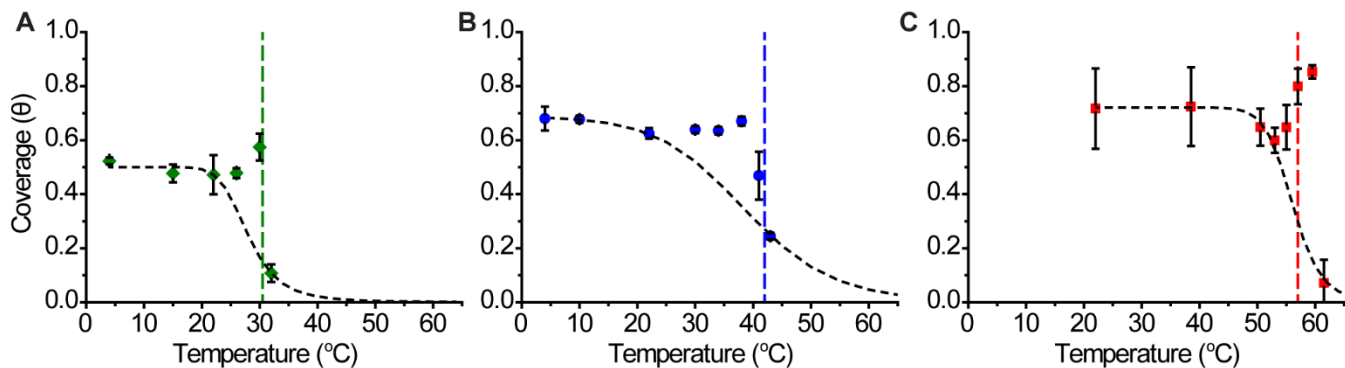
Figure 4. Coverage dependence on temperature for three systems: green is the standard sticky end in 0.15 M PBS, blue is the standard sticky end in 0.5 M PBS, and red is the long sticky end in 0.5 M PBS. Vertical lines show each system's respective melting temperatures, black curves show a representative fit to the Langmuir model. Error bars are 95% confidence intervals.

Neither the standard RSA model nor the Langmuir model can account for this reorganization behavior, but extensions to both models can qualitatively explain the trends. A straightforward extension to the Langmuir model can predict the equilibrium coverage increase at higher temperatures by including a term for inaccessible sites (θ_{bl}) that become available for adsorption as particles become mobile (see SI). The equilibrium equation then becomes

$$k_{des}\theta = k_{ads}P(1-\theta-\theta_{bl}) \qquad (7)$$

where θ_{bl} is temperature dependent, decreasing at elevated temperatures (see eq S10). However, while this simple extension to the model is fairly intuitive and shows the correct curve shape, it does not contain enough free parameters to fit the system quantitatively. This is because the model does not account for the amount of interparticle repulsion or variation in PAE mobility as a function of coverage. As more PAEs land on the surface, the energy for adsorption and rearrangement would be expected to increase, leading to decreasing mobility. Other modifications to the Langmuir model account for coverage-dependent adsorption energy and interparticle repulsion[43] (the Hill-deBoer equation, eq S6), but require iterative methods to solve. As they do

not provide significant insight into the reorganization process or specific mechanisms of PAE reorganization on the surface, they are not discussed here.

With the RSA model, altering the simulation parameters to allow for diffusion causes the equilibrium surface coverage to eventually reach the close-packed state of 0.906, consisting of a hexagonal lattice of particles[44]. The simulation results of this prior work imply that it should theoretically be possible to tune the PAE system to have highly mobile particles that will reach a close-packed state in an experimentally achievable timeframe[45,46]. Nevertheless, as mentioned above, the RSA model utilizes complex numerical methods to simulate deposition and thus will be the focus of future works. However, we can still examine this behavior experimentally through identifying changes to the film morphology; as particles become mobile, the morphology of the thin film should transition from a random arrangement to one that contains more ordering.

Morphology of the Deposited Monolayers

The UV-Vis experiments above show that it is possible to modulate surface coverage by altering either the PAE design or the concentration of counterions in solution. However, they do not provide any information on the overall morphology of the films. It is possible that two films could have the same coverage as measured by UV-Vis spectroscopy (i.e. the same number of particles have deposited on the surface) but completely different arrangements of those particles in the 2D monolayer. Further analysis with SEM imaging of the substrates was therefore conducted to determine if the experimental variables of solution ionic strength, sticky end binding strength, and temperature had significant impact on the arrangement of particles on the deposited surface.

Interparticle distances and overall surface morphology were analyzed using small-angle X-ray scattering (SAXS) spectra of representative substrates (Figures S11 and S12), as well as radial

distribution function (RDF) analysis of SEM images (Figures 5 and S10). Both sets of data demonstrate that, as temperature increases, the previously hypothesized reorganization of PAEs during deposition leads to monolayers that contain more short-range ordering, ultimately leading to a "liquid phase" where nanoparticles can be found at random locations but with a consistent interparticle distance. Order analysis was also performed by determining the number of nearest neighbors for each PAE through a Voronoi analysis of the SEM images, showing that the average coordination number of each PAE approaches six as the temperature of a system increases, transitioning towards a hexatic monolayer (Figure S8 and S9). The greater extent of ordering in the system is attributed to the overall rate of binding and unbinding events increasing in magnitude when deposition is conducted at higher temperatures. By increasing the absolute rate of these binding and unbinding events, PAEs are able to sample a larger number of surface states. This drives the PAEs to locations that maximize overall PAE-surface binding, lowering the overall system energy, ultimately leading to the observed quasihexagonal particle arrangement. This means that, regardless of other design factors, higher deposition temperatures lead to more liquid-phase-like behavior and an increased amount of order. Because the equilibrium surface coverage can be shifted with the PAE design, solution ion concentration, and temperature, proper manipulation of these factors allows for independent control over the number of particles on the surface and their overall arrangement and degree of ordering (Figure 5).
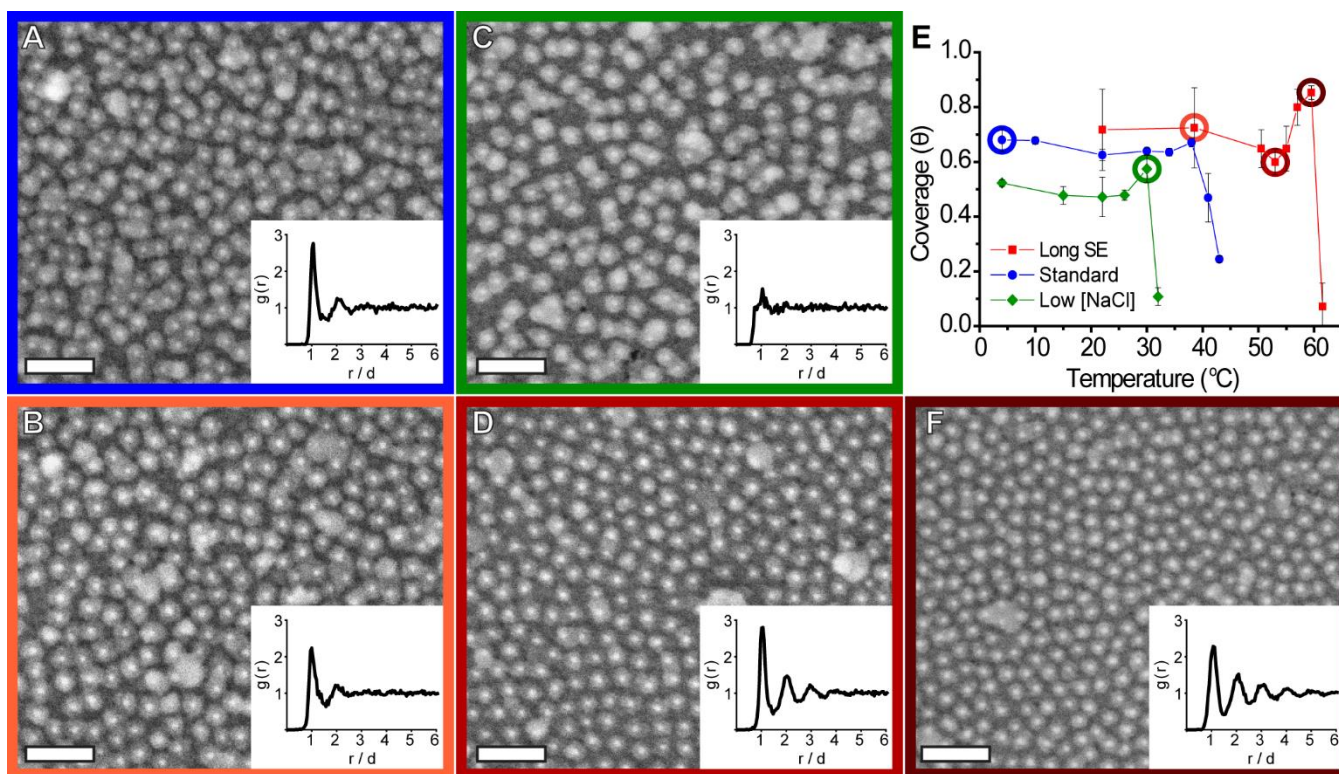
Figure 5. Coverage and morphology change as a function of PAE design and deposition conditions. As temperature increases (B→D→F), particles become more uniformly distributed (inset RDF). Additionally, surface coverage and morphology can be independently controlled, as two systems can be deposited to have the same macroscopic density but either identical (A and B) or different (C and D) particle arrangements. Circled data points in E correspond to the images with the same outline colors. Scale bars are 200 nm.

Morphology control of Bilayer and Multilayer Films

Because many applications involving nanoparticle thin films require multiple layers of particles[7,13], additional experiments were undertaken to understand how the modifications to the morphology of the first layer affected subsequent rounds of particle deposition. To achieve these multilayer films, additional particle layers were deposited by first incubating the monolayer-coated substrate in a batch of nanoparticles functionalized with a sticky end that was complementary to

the first layer (i.e. linkers with the same sticky end as the substrate). Subsequent layers were deposited by sequentially immersing the substrate in alternating solutions of the two complementary PAE types to achieve films of the desired thickness. The thermodynamic equilibrium of this binary PAE system has been shown to be a bcc lattice oriented with the {100} planes parallel to the surface[5]. However, achieving these ordered superlattice architectures requires thermal annealing; PAE aggregates formed at room temperature typically exhibit only short-range ordering and no crystallinity. It was therefore hypothesized that a second layer of PAEs deposited at room temperature would not have the thermal energy to cause the first layer to rearrange, resulting in an amorphous film. Conversely, depositing PAEs at an elevated temperature near the melting temperature would allow formation of the bcc structure. As predicted, when the second layer is deposited at room temperature, the resulting structure appears to have an amorphous, incomplete layer, regardless of the deposition conditions of the initial monolayer. However, AFM images confirm that deposition of a second layer at elevated temperatures leads to a polycrystalline structure with {100} planes parallel to the substrate (Figure 6), indicating that the addition of a second layer induced reorganization of the initially deposited PAEs. Interestingly, when the first layer was deposited at low solution ionic strength (resulting in low surface coverage), but the second layer was deposited in 0.5 M PBS at high temperature, bcc lattices were still observed, but the resulting thin film formed crystalline patches rather than a complete film (Figure 6C), as there were not enough PAEs in the initial monolayer to fully form a bilayer crystal across the entire substrate. These results indicate that it is possible to control film morphology and surface coverage of multilayer films in a rational manner, with the potential to use this controllable architecture to make thick films with minimal surface roughness.
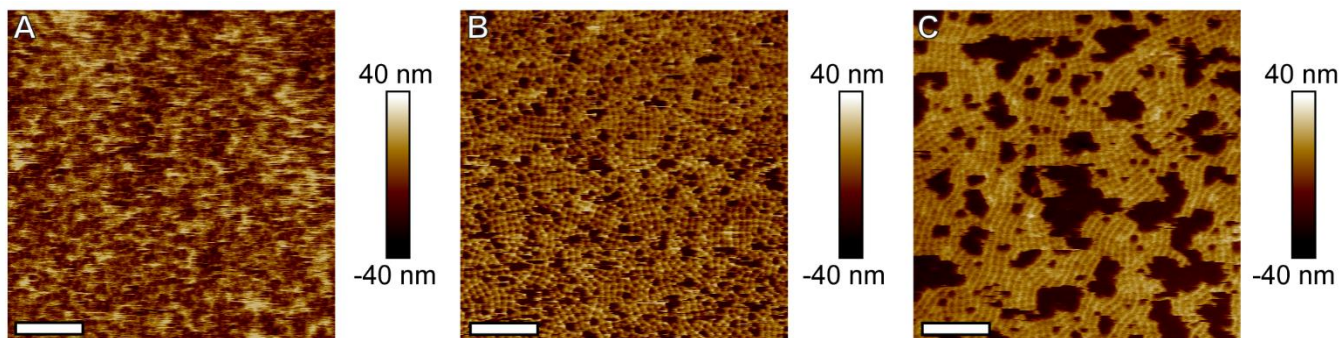
Figure 6. Bilayer morphology can be altered by deposition under different conditions. (A) amorphous layer from 22 °C deposition, (B) crystalline film from deposition at 39 °C, and (C) a patchy crystalline film achieved through first layer deposition in low ionic strength solution (resulting in low coverage). Scale bars are 500 nm.

To examine the possibility of using initial deposition conditions to better control thin film morphology in multilayer samples, five layer films were produced at the optimum deposition conditions (those that produced the highest coverage) for each of the three systems studied (low ionic strength, standard, and long sticky end). AFM images were taken to determine average roughness and grain size for each of these deposition protocols (Figure 7). Just as was observed in the monolayer and bilayer systems, the low ionic strength deposition conditions resulted in lower coverage—in multilayer films, this translated into the growth of isolated patches of PAE crystals, yielding highly rough (R_q = 41.5 nm) and discontinuous thin films with small islands on the order of 280 nm in diameter. In contrast, both the standard case and the long sticky end case produced smooth crystalline thin films with surface roughnesses (R_q) of 18.9 nm and 14.1 nm respectively. The standard system produced the largest grain size, on average 667 nm diameter (~ 9 x 9 bcc array of PAEs), while the long sticky end produced smaller grains on the order of 525 nm diameter (~7 x 7 bcc array of PAEs). It is hypothesized that the standard system exhibited nominally larger grain size and higher surface roughness than the long sticky end system due to a slightly lower

initial surface coverage, leading to increased migration of nanoparticles in the initial layer that would allow larger grains to form, but leave gaps that must be filled in with later layers.
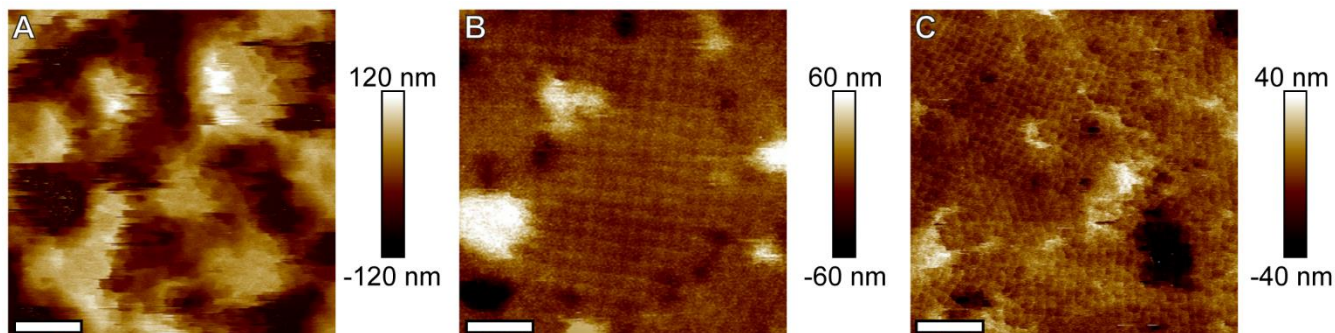
Figure 7. AFM images of five-layer films. Note that the low ionic strength case (A) yields rough, discontinuous thin film, while the standard case (B) produces large crystalline grains, and the long sticky end case (C) produces smaller grains but with even lower surface roughness (height scales are different between the three images). Scale bars are 300 nm.

Conclusions

Colloidal deposition commonly occurs through electrostatic interactions or interfacial forces, however these methods lack precise control over the structure and ordering of the surface. While ionic strength can control the surface coverage with electrostatic interactions in those systems, the interparticle repulsive forces cannot be decoupled from the attractive potential to the surface. In contrast, PAEs utilize complementary binding that can independently control the affinity of particles to the surface while tuning the electrostatic interactions between particles. This system therefore enables precise control over the surface coverage and thin film morphology, and also allows for layer-by-layer deposition of complementary particle types, facilitating the growth of crystalline thin films.

We have demonstrated the ability to tune surface coverage through the interplay of solution ion concentration, temperature, and PAE design. In addition, we have shown that at a particular surface

coverage, the morphology of the PAE thin film can be modulated to achieve short-range ordering, even without attractive interactions between individual particles. Extending this knowledge to multiple layers allows us to tailor the structure of these thin films from amorphous to polycrystalline and to alter the grain size and surface roughness at will. This remarkable programmability of the surface morphology lends itself to many applications, including colloidal templating and tailoring of interfacial phenomena (e.g. cell-surface interactions, hydrophobicity, or catalysis).

ASSOCIATED CONTENT

Supporting Information. Experimental procedures, including oligonucleotide sequences, nanoparticle functionalization and assembly, substrate preparation, and characterization/analysis techniques (SEM, SAXS, and AFM) are available in the SI. Additional experiments and calculations can also be found in the SI.

AUTHOR INFORMATION

Corresponding Author

*rmacfarl@mit.edu

Author Contributions

The manuscript was written through contributions of all authors. All authors have given approval to the final version of the manuscript.

ABBREVIATIONS

REFERENCES

(1) Pincella, F.; Isozaki, K.; Miki, K. A Visible Light-Driven Plasmonic Photocatalyst. *Light Sci. Amp Appl.* **2014**, *3*, e133.
(2) Liu, X.; Du, X.; He, J. Hierarchically Structured Porous Films of Silica Hollow Spheres via Layer-by-Layer Assembly and Their Superhydrophilic and Antifogging Properties. *ChemPhysChem 9* (2), 305–309.
(3) Lee, D.; Rubner, M. F.; Cohen, R. E. All-Nanoparticle Thin-Film Coatings. *Nano Lett.* **2006**, *6* (10), 2305–2312.

(4)   Spadavecchia, J.; Prete, P.; Lovergine, N.; Tapfer, L.; Rella, R. Au Nanoparticles Prepared by Physical Method on Si and Sapphire Substrates for Biosensor Applications. *J. Phys. Chem. B* **2005**, *109* (37), 17347–17349.

(5)   Senesi, A. J.; Eichelsdoerfer, D. J.; Macfarlane, R. J.; Jones, M. R.; Auyeung, E.; Lee, B.; Mirkin, C. A. Stepwise Evolution of DNA-Programmable Nanoparticle Superlattices. *Angew. Chem. Int. Ed.* **2013**, *52* (26), 6624–6628.

(6)   Phillips, K. R.; England, G. T.; Sunny, S.; Shirman, E.; Shirman, T.; Vogel, N.; Aizenberg, J. A Colloidoscope of Colloid-Based Porous Materials and Their Uses. *Chem Soc Rev* **2016**, *45* (2), 281–322.

(7)   Richardson, J. J.; Bjornmalm, M.; Caruso, F. Technology-Driven Layer-by-Layer Assembly of Nanofilms. *Science* **2015**, *348* (6233), aaa2491–aaa2491.

(8)   Zhang, J.; Li, Y.; Zhang, X.; Yang, B. Colloidal Self-Assembly Meets Nanofabrication: From Two-Dimensional Colloidal Crystals to Nanostructure Arrays. *Adv. Mater.* 22 (38), 4249–4269.

(9)   Tao, A.; Sinsermsuksakul, P.; Yang, P. Tunable Plasmonic Lattices of Silver Nanocrystals. *Nat. Nanotechnol.* **2007**, *2*, 435.

(10)   Vogel, N.; Weiss, C. K.; Landfester, K. From Soft to Hard: The Generation of Functional and Complex Colloidal Monolayers for Nanolithography. *Soft Matter* **2012**, *8* (15), 4044–4061.

(11)   Shevchenko, E. V.; Talapin, D. V.; Kotov, N. A.; O'Brien, S.; Murray, C. B. Structural Diversity in Binary Nanoparticle Superlattices. *Nature* **2006**, *439*, 55.

(12)   Kalsin, A. M.; Fialkowski, M.; Paszewski, M.; Smoukov, S. K.; Bishop, K. J. M.; Grzybowski, B. A. Electrostatic Self-Assembly of Binary Nanoparticle Crystals with a Diamond-Like Lattice. *Science* **2006**, *312* (5772), 420–424.

(13)   Jones, M. R.; Osberg, K. D.; Macfarlane, R. J.; Langille, M. R.; Mirkin, C. A. Templated Techniques for the Synthesis and Assembly of Plasmonic Nanostructures. *Chem. Rev.* **2011**, *111* (6), 3736–3827.

(14)   Ye, X.; Zhu, C.; Ercius, P.; Raja, S. N.; He, B.; Jones, M. R.; Hauwiller, M. R.; Liu, Y.; Xu, T.; Alivisatos, A. P. Structural Diversity in Binary Superlattices Self-Assembled from Polymer-Grafted Nanocrystals. *Nat. Commun.* **2015**, *6*, 10052.

(15)   Gabrys, P. A.; Seo, S. E.; Wang, M. X.; Oh, E.; Macfarlane, R. J.; Mirkin, C. A. Lattice Mismatch in Crystalline Nanoparticle Thin Films. *Nano Lett.* **2018**, *18* (1), 579–585.

(16)   Macfarlane, R. J.; Lee, B.; Jones, M. R.; Harris, N.; Schatz, G. C.; Mirkin, C. A. Nanoparticle Superlattice Engineering with DNA. *science* **2011**, *334* (6053), 204–208.

(17)   Macfarlane, R. J.; Jones, M. R.; Lee, B.; Auyeung, E.; Mirkin, C. A. Topotactic Interconversion of Nanoparticle Superlattices. *Science* **2013**, *341* (6151), 1222–1225.

(18)   O'Brien, M. N.; Jones, M. R.; Lee, B.; Mirkin, C. A. Anisotropic Nanoparticle Complementarity in DNA-Mediated Co-Crystallization. *Nat. Mater.* **2015**, *14* (8), 833–839.

(19)   Nykypanchuk, D.; Maye, M. M.; van der Lelie, D.; Gang, O. DNA-Guided Crystallization of Colloidal Nanoparticles. *Nature* **2008**, *451* (7178), 549–552.

(20)   Valignat, M.-P.; Theodoly, O.; Crocker, J. C.; Russel, W. B.; Chaikin, P. M. Reversible Self-Assembly and Directed Assembly of DNA-Linked Micrometer-Sized Colloids. *Proc. Natl. Acad. Sci. U. S. A.* **2005**, *102* (12), 4225–4229.

(21)   Wang, Y.; Wang, Y.; Zheng, X.; Ducrot, É.; Yodh, J. S.; Weck, M.; Pine, D. J. Crystallization of DNA-Coated Colloids. *Nat. Commun.* **2015**, *6*, 7253.

(22) Ku, J. C.; Ross, M. B.; Schatz, G. C.; Mirkin, C. A. Conformal, Macroscopic Crystalline Nanoparticle Sheets Assembled with DNA. *Adv. Mater.* **2015**, *27* (20), 3159–3163.

(23) Shim, T. S.; Estephan, Z. G.; Qian, Z.; Prosser, J. H.; Lee, S. Y.; Chenoweth, D. M.; Lee, D.; Park, S.-J.; Crocker, J. C. Shape Changing Thin Films Powered by DNA Hybridization. *Nat. Nanotechnol.* **2016**, *12* (1), 41–47.

(24) Myers, B. D.; Lin, Q.-Y.; Wu, H.; Luijten, E.; Mirkin, C. A.; Dravid, V. P. Size-Selective Nanoparticle Assembly on Substrates by DNA Density Patterning. *ACS Nano* **2016**, *10* (6), 5679–5686.

(25) Wang, M. X.; Seo, S. E.; Gabrys, P. A.; Fleischman, D.; Lee, B.; Kim, Y.; Atwater, H. A.; Macfarlane, R. J.; Mirkin, C. A. Epitaxy: Programmable Atom Equivalents *Versus* Atoms. *ACS Nano* **2017**, *11* (1), 180–185.

(26) Bastús, N. G.; Comenge, J.; Puntes, V. Kinetically Controlled Seeded Growth Synthesis of Citrate-Stabilized Gold Nanoparticles of up to 200 Nm: Size Focusing versus Ostwald Ripening. *Langmuir* **2011**, *27* (17), 11098–11105.

(27) Hill, H. D.; Mirkin, C. A. The Bio-Barcode Assay for the Detection of Protein and Nucleic Acid Targets Using DTT-Induced Ligand Exchange. *Nat. Protoc.* **2006**, *1*, 324.

(28) Auyeung, E.; Macfarlane, R. J.; Choi, C. H. J.; Cutler, J. I.; Mirkin, C. A. Transitioning DNA-Engineered Nanoparticle Superlattices from Solution to the Solid State. *Adv. Mater.* *24* (38), 5181–5186.

(29) Macfarlane, R. J.; Thaner, R. V.; Brown, K. A.; Zhang, J.; Lee, B.; Nguyen, S. T.; Mirkin, C. A. Importance of the DNA "Bond" in Programmable Nanoparticle Crystallization. *Proc. Natl. Acad. Sci.* **2014**, *111* (42), 14995–15000.

(30) O'Brien, M. N.; Radha, B.; Brown, K. A.; Jones, M. R.; Mirkin, C. A. Langmuir Analysis of Nanoparticle Polyvalency in DNA-Mediated Adsorption. *Angew. Chem. Int. Ed.* **2014**, *53* (36), 9532–9538.

(31) Langmuir, I. THE ADSORPTION OF GASES ON PLANE SURFACES OF GLASS, MICA AND PLATINUM. *J. Am. Chem. Soc.* **1918**, *40* (9), 1361–1403.

(32) Macfarlane, R. J.; Jones, M. R.; Senesi, A. J.; Young, K. L.; Lee, B.; Wu, J.; Mirkin, C. A. Establishing the Design Rules for DNA-Mediated Programmable Colloidal Crystallization. *Angew. Chem.* **2010**, *122* (27), 4693–4696.

(33) Bloomfield, V. A.; Crothers, D. M.; Tinoco, I. *Nucleic Acids: Structure, Properties, and Functions*; University Science Books, 2000.

(34) Talbot, J.; Tarjus, G.; Van Tassel, P. R.; Viot, P. From Car Parking to Protein Adsorption: An Overview of Sequential Adsorption Processes. *Colloids Surf. Physicochem. Eng. Asp.* **2000**, *165* (1–3), 287–324.

(35) Adamczyk, Z.; Nattich-Rak, M.; Sadowska, M.; Michna, A.; Szczepaniak, K. Mechanisms of Nanoparticle and Bioparticle Deposition – Kinetic Aspects. *Colloids Surf. Physicochem. Eng. Asp.* **2013**, *439*, 3–22.

(36) Hinrichsen, E. L.; Feder, J.; Jøssang, T. Geometry of Random Sequential Adsorption. *J. Stat. Phys.* **1986**, *44* (5), 793–827.

(37) Semmler, M.; Rička, J.; Borkovec, M. Diffusional Deposition of Colloidal Particles: Electrostatic Interaction and Size Polydispersity Effects. *Colloids Surf. Physicochem. Eng. Asp.* **2000**, *165* (1–3), 79–93.

(38) Adamczyk, Z.; Siwek, B.; Zembala, M.; Weroński, P. Influence of Polydispersity on Random Sequential Adsorption of Spherical Particles. *J. Colloid Interface Sci.* **1997**, *185* (1), 236–244.

(39) Kewalramani, S.; Guerrero-García, G. I.; Moreau, L. M.; Zwanikken, J. W.; Mirkin, C. A.; Olvera de la Cruz, M.; Bedzyk, M. J. Electrolyte-Mediated Assembly of Charged Nanoparticles. *ACS Cent. Sci.* **2016**, *2* (4), 219–224.

(40) Seo, S. E.; Li, T.; Senesi, A. J.; Mirkin, C. A.; Lee, B. The Role of Repulsion in Colloidal Crystal Engineering with DNA. *J. Am. Chem. Soc.* **2017**, *139* (46), 16528–16535.

(41) Hanarp, P.; Sutherland, D. S.; Gold, J.; Kasemo, B. Control of Nanoparticle Film Structure for Colloidal Lithography. *Colloids Surf. Physicochem. Eng. Asp.* **2003**, *214* (1–3), 23–36.

(42) Brouwer, E. A. M.; Kooij, E. S.; Hakbijl, M.; Wormeester, H.; Poelsema, B. Deposition Kinetics of Nanocolloidal Gold Particles. *Colloids Surf. Physicochem. Eng. Asp.* **2005**, *267* (1–3), 133–138.

(43) Sircar, S.; Myers, A. L. Equilibrium Adsorption of Gases and Liquids on Heterogeneous Adsorbents — A Practical Viewpoint. *Surf. Sci.* **1988**, *205* (3), 353–386.

(44) Watanabe, S.; Miyahara, M.; Higashitani, K. Dynamics of Order Formation by Colloidal Adsorption onto a Substrate Studied with Brownian Dynamics. *J. Chem. Phys.* **2005**, *122* (10), 104704.

(45) Miyahara, M.; Watanabe, S.; Gotoh, Y.; Higashitani, K. Adsorption and Order Formation of Colloidal Nanoparticles on a Substrate: A Brownian Dynamics Study. *J. Chem. Phys.* **2004**, *120* (3), 1524–1534.

(46) Gray, J. J.; Bonnecaze, R. T. Adsorption of Colloidal Particles by Brownian Dynamics Simulation: Kinetics and Surface Structures. *J. Chem. Phys.* **2001**, *114* (3), 1366–1381.

For Table of Contents Only